Circulation (AMOC), so-called $T_{AMOC}$, and some of its components. When the AMOC transport is small, the mean sea surface height of the Mediterranean Sea is high. In addition, in this work we show that the $MSSH_{MS}$ is correlated with the Gibraltar inflow transport, $F_{inflow,}$ which is representative of the upper branch of the Mediterranean Zonal Overturning Circulation.

The novel result here is to show a clear anti-correlation between the $T_{AMOC}$ and its components with $F_{inflow}$ at interannual time scales, which has never been discussed before. We argue that the wind-driven induced changes in the North Atlantic are responsible not only for the AMOC variability but largely also for the variability of the Gibraltar inflow transport through Azores Current changes and ultimately to the Mediterranean Sea overturning circulation.

We show that during years of weaker/stronger AMOC and higher/lower SSH in the Mediterranean, stronger/weaker Azores Current reflects into stronger/weaker Gibraltar inflow transport. The direct wind driven mechanism suggested by Volkov et al. (2019) for the AMOC is instead indirect on the Mediterranean Sea mean SSH, producing first a changed Gibraltar transport which in turn produces a change in Mediterranean Sea SSH.

The correlations have maximum values at different time lags, but these depend on the specific time period used for the analysis and we expect these values to have large uncertainties. Limitations to our analysis are inherent to the short time series (1993–2019) since decadal variability cannot be resolved by the 27-year period.

In conclusion, we have connected for the first time the integrated transport of the AMOC with the Mediterranean Sea Gibraltar transport and suggested that the Azores Current plays an important role. We believe this correlation could be of great importance in the future climate scenarios where the North Atlantic is undergoing major changes due to Greenland ice melting and changes in the wind forcing. Future work should consider extending this analysis to longer time series in order to be able to discern the longer time scale correlations.

## Section 2.6. Winter fertilization in the Mediterranean Sea euphotic layer and its relationship with Northern Hemisphere large-scale circulation patterns

**Authors:** Marco Reale, Gianpiero Cossarini, Stefano Salon, Valeria Di Biagio, Anna Teruzzi, Gianluca Coidessa, Emanuela Clementi

**Statement of main outcomes:** The fertilization of the Mediterranean Sea euphotic layer during winter, as a result, for example, of strong vertical mixing driven by the air–sea interaction, acts in the direction of mitigating the overall oligotrophic state of the basin, influencing at the same time the size distribution of phytoplankton and the food webs in the marine ecosystems of the basin. Here we introduce marine trophic state indicators based on the climatological 90th percentile of daily winter concentration of nutrients to assess locally the potential fertilization of the euphotic layer and its link to Northern Hemisphere large-scale circulation patterns. We found that potential fertilization in the Western (Eastern) Mediterranean is predominantly linked to negative (positive) states of the East Atlantic (East Atlantic/Western Russian) patterns that shape the heat flux losses at the ocean surface and the associated vertical mixing.

**Products used:**

| Ref. No. | Product name & type | Documentation |
|---|---|---|
| 2.6.1 | MEDSEA_MULTIYEAR_PHY_006_004 | https://marine.copernicus.eu/documents/QUID/CMEMS-MED-QUID-006-004.pdf https://marine.copernicus.eu/documents/PUM/CMEMS-MED-PUM-006-004.pdf |
| 2.6.2 | MEDSEA_MULTIYEAR_BGC_006_008 | https://catalogue.marine.copernicus.eu/documents/QUID/CMEMS-MED-QUID-006-008.pdf https://catalogue.marine.copernicus.eu/documents/PUM/CMEMS-MED-PUM-006-008.pdf |
| 2.6.3 | Time series of the monthly values of the indexes for large-scale circulation patterns used in the present contribution are available at NOAA climate prediction centre | https://www.cpc.ncep.noaa.gov/data/teledoc/telecontents.shtml |

### 2.6.1. Introduction

The Mediterranean Sea is widely recognised as an oligotrophic basin (ultra-oligotrophic in the Eastern part), thus characterised by low levels of nutrients concentration (e.g., $PO_4$ and $NO_3$) and integrated net primary production compared to the global ocean and a characteristic east–west trophic gradient (Moutin and Raimbault 2002; Siokou-Frangou et al. 2010; Lazzari et al. 2012; Di Biagio et al. 2019; Reale et al. 2020a). These features result from the overlapping of different physical and biogeochemical processes, such as the anti-estuarine circulation at the Gibraltar Strait, the biological pump in the basin, water column stratification and the

spatial distribution of phytoplankton-limiting growth nutrient (e.g. $PO_4$ and $NO_3$) sources (Crise et al. 1999; Crispi et al. 2001; Huertas et al. 2012).

In some areas of the basin the oligotrophic state is occasionally mitigated (typically in winter) by the injection of dissolved nutrients in the euphotic layer from the deep waters, as a consequence, for example, of strong mixing mostly driven by heat losses and wind forcing stress acting at the sea surface (Reale et al. 2020b). This 'fertilization' of the water column in winter acts to favour a decrease of the overall oligotrophy of the basin (Siokou-Frangou et al. 2010).

Over the last years, different indicators have been developed to assess the eutrophication of the European regional basins based on satellite-derived 90th percentile of the daily value of chlorophyll-a concentrations (see Gohin et al. 2019; Pardo et al. 2021 for a review). On the other hand, indicators evaluating the fertilization of the euphotic layer in winter and the relationship between these indicators and the large-scale circulation patterns driving the physical forcing acting on the water column (Josey et al. 2011; Papadopoulos et al. 2012; Ulbrich et al. 2012; Reale et al. 2020b) are still poorly investigated. Should this relationship be established, it could pave the way to develop seasonal forecasts of the eutrophication tendency in the basin.

In this work, we first introduce two 'potential fertilization indicators', defined in each point of the Mediterranean Sea, for each of the most relevant limiting nutrients for phytoplankton growth ($PO_4$ and $NO_3$), based on their climatological daily winter 90th percentile (hereafter: 90th). Secondly, we associate the indicators with the temporal variability of the main Northern Hemisphere large-scale circulation patterns (North Atlantic Oscillation, East Atlantic, East Atlantic/Western Russia and Scandinavian pattern). Thirdly, we discuss the possibility of using the established link to develop seasonal forecasts for the eutrophication tendencies in some areas of the basin.

## 2.6.2. Materials and methods

We derived the 'potential fertilization indicators' for dissolved nutrients in the Mediterranean Sea using 3D daily $PO_4$ and $NO_3$ fields provided by the 1999–2019 CMEMS biogeochemical reanalysis at 1/24° horizontal resolution and 125 vertical levels (MEDSEA_MULTIYEAR_BGC_006_008, product reference 2.6.2). The CMEMS biogeochemical reanalysis is produced by the OGSTM-BFM-3DVarBio model (Salon et al. 2019; Cossarini et al. 2021; Teruzzi et al. 2021) coupled off-line with the physical NEMO-OceanVar model (Escudier et al. 2021) that is forced with ERA5 atmospheric fields. The biogeochemical reanalysis assimilates surface chlorophyll-a estimates from satellite ocean colour while NEMO-OceanVar model assimilates satellite sea surface height and in-situ profiles of temperature and salinity (MEDSEA_MULTIYEAR_PHY_006_004, product reference 2.6.1). The two reanalyses have been extensively validated (Cossarini et al. 2021; Escudier et al. 2021) following the CMEMS product quality standard guidelines (Hernandez et al. 2018).

Recently, several indicators to assess the eutrophic state of the mid-latitude lakes or ocean basins were developed using different percentile thresholds (75th, 90th, 95th) of the daily values distribution computed for the entire water bodies or locally in each point of the basin (e.g. Poikāne et al. 2010; Desmit et al. 2018; Gohin et al. 2019; Greenwood et al. 2019; Brito et al. 2020; Pardo et al. 2021). Here we use the 90th percentile as a measure of the richness in nutrients or fertilization of the euphotic layer in each point of the domain before the onset of stratified spring conditions, which lead to the phytoplankton blooms. Although arbitrary, the 90th percentile has been chosen in several other studies to characterise the mid-latitude basins eutrophic state (Desmit et al. 2018; Gohin et al. 2019; Pardo et al. 2021).

In order to compute the climatological 90th percentile we first averaged the concentration of both nutrients over the first 100 m of the water column, which can be considered approximately the thickness of the euphotic layer in the basin. Secondly, we considered in each grid point of the domain the 90th percentile of the daily winter concentration of $PO_4$ and $NO_3$ (hereafter: $90th_{PO4}$ and $90th_{NO3}$) in the period 1999–2019, where winter corresponds to December, January and February (hereafter: DJF). The 90th percentile threshold is calculated in each point of the basin in order to evaluate the potential fertilization in relation to the local mean trophic level, as recently proposed for local extreme events in Di Biagio et al. (2020).

Then, we defined for each point of the basin a 'potential fertilization indicator' for $PO_4$ and $NO_3$ (hereafter: $FE_{PO4}$ and $FE_{NO3}$) as the number of days (not necessarily consecutive) in each winter month of the period 1999–2019 when the value of $PO_4$ and $NO_3$ is greater than $90th_{PO4}$ and $90th_{NO3}$, respectively. In this work the term 'fertilization' refers to the accumulation of phytoplankton limiting-growth nutrients in the euphotic layer because of different processes acting locally such as input (e.g. vertical mixing, riverine input) or lack of consumption. The higher is the value of the index, the more efficient are these processes to accumulate the dissolved nutrients in the euphotic layer. On the other hand, the adjective 'potential' refers to the fact that the presence of high values of nutrients in the euphotic

layer is a necessary but not sufficient condition for the development of the phytoplankton blooms. In fact, beside the nutrient content of the euphotic layer, other processes may impact the intensity and temporal evolution of the spring blooms (Mayot et al. 2017).

This formulation allows us to investigate whether the highest values of both $FE_{PO4}$ and $FE_{NO3}$ at each point of the basin could correspond to a particular state of the Northern Hemisphere large-scale atmospheric circulation patterns which shape heat fluxes and, in turn, the vertical mixing in the basin, which is one of the main drivers of the nutrients' dynamics in the euphotic layer (Josey et al. 2011; Papadopoulos et al. 2012; Reale et al. 2020b).

In this work, in order to characterise the temporal variability of large-scale circulation patterns we use their available monthly indexes that are standardised with respect to the climatology of 1981–2010 (product reference 2.6.3). The large-scale circulation patterns here considered are: North Atlantic Oscillation (NAO), East Atlantic (EA), East Atlantic/Western Russian (EAWR) and Scandinavian pattern (SCAN), which have been widely recognised as important drivers of the physical forcing and of the biogeochemical dynamics of the Mediterranean basin in winter (Josey et al. 2011; Papadopoulos et al. 2012; Ulbrich et al. 2012; Reale et al. 2020b).

In order to investigate at which extent the highest monthly values of $FE_{PO4}$ and $FE_{NO3}$ in each point of the basin correspond to a particular large-scale circulation pattern monthly state, we selected all those winter months when $FE_{PO4}$ and $FE_{NO3}$ are greater than seven and computed the mean values of the four large-scale circulation patterns indexes for those months (hereafter: $SP^{+}$). The threshold of seven days per month has been chosen after a sensitivity analysis of the statistical significance of the relationship between large-scale circulation patterns and the potential fertilization indicators (not shown).

Finally, we assessed if these values are statistically different from the climatological means of the four indexes during the winter months (SPclim). The statistical significance of the observed difference of the two means have been assessed using a Mann–Whitney test with $p < 0.05$.

### 2.6.3. Results

Figure 2.6.1 shows the spatial distribution in the Mediterranean Sea of $90th_{PO4}$ and $90th_{NO3}$ percentile in DJF during the period 1999–2019. The distribution is characterised by an east–west/south–north gradient for $PO_4/NO_3$ whose existence has been already pointed out in previous works (Crise et al. 1999; Manca et al. 2004; Lazzari et al. 2016; Richon et al. 2018a, 2018b; Di Biagio et al. 2019; Richon et al. 2019; Reale et al. 2020a, 2020b). The highest values are observed in the deep convective areas of the basin, namely the Gulf of Lion, Southern Adriatic Sea and the area of Rhodes Gyre (Macias et al. 2018b). Moreover, additional strong signals can be found in the Alboran Sea, associated with the coastal upwelling and inflow of Atlantic water at the Gibraltar Strait (Macias et al. 2018a), in the Northern Ionian as a consequence of the deepening of the mixed layer depth in the area in winter (D'Ortenzio et al. 2005; Lavigne et al. 2018), in the area of Northern Tyrrhenian, Pelops and Shikmona gyres (Pinardi et al. 2015) and along the coastlines of the basin, for example in the area of Rhone and Ebro river plumes (Western Mediterranean Sea), in the Northern Adriatic Sea (Po river) and in the Levantine basin at the mouth of the Nile river. The Mediterranean riverine inputs are characterised by high values of the N:P ratio (Lazzari et al. 2016), thus explaining the higher $NO_3$ concentrations near the river mouths which are, at least, more than one order of magnitude greater with respect to what is observed in the case of $PO_4$.

During the winter season, the highest values of FE for both nutrients are observed mainly in February in the offshore areas of the basin when the mixed layer depth

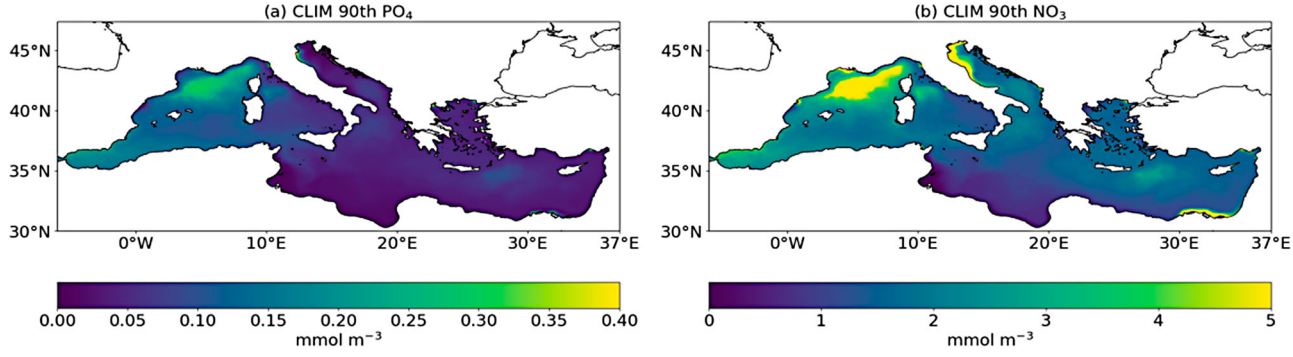


**Figure 2.6.1.** Spatial distribution of $90th_{PO4}$ (a) and $90th_{NO3}$ (b) percentile in the Mediterranean Sea in DJF (period 1999–2019). Values in both panels are in mmol/$m^3$ and have been computed using the CMEMS biogeochemical reanalysis (product reference 2.6.2)

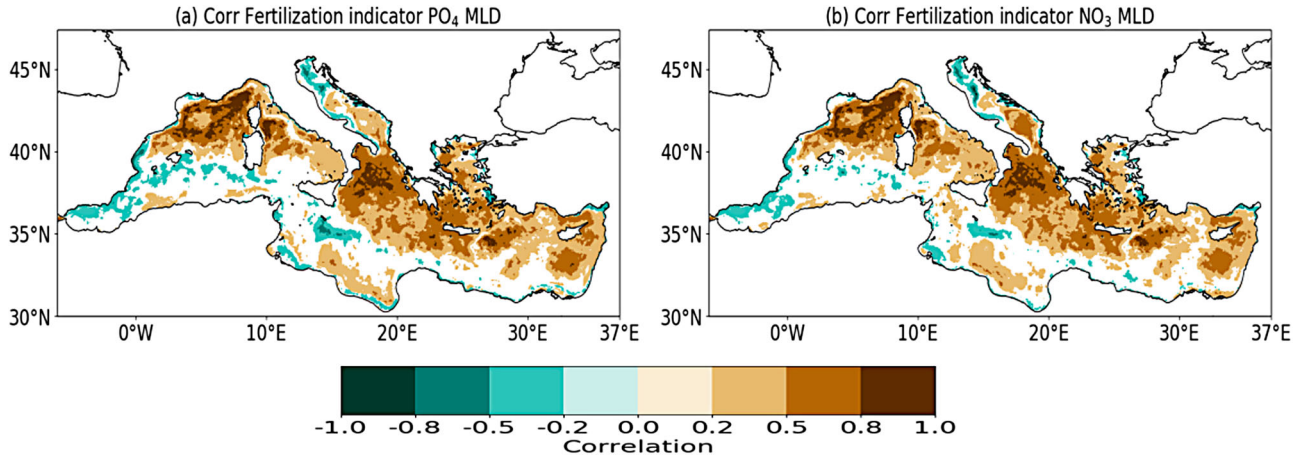


**Figure 2.6.2.** Spatial distribution of the correlation between the monthly DJF winter time series of the mixed layer depth and $FE_{PO4}$ (a) and $FE_{NO3}$ (b) respectively in the period 1999–2019. Only correlation values statistically significant at 95% are shown. Mixed layer depth data are based on the CMEMS physical reanalysis (product reference 2.6.1). $FE_{PO4}$ and $FE_{NO3}$ have been calculated using the CMEMS biogeochemical reanalysis (product reference 2.6.2).

in the basin is at its maximum (D'Ortenzio et al. 2005; Houpert et al. 2015), whilst relatively lower values occur at the river mouths (such as the Po and Nile), in the Gulf of Gabes and in the Alboran Sea. In this case vertical mixing plays a twofold role: (i) it enriches nutrients in the euphotic layer eroding the nutricline; and (ii) it prevents concentration of phytoplankton at the surface by dilution. Moreover, sunlight is minimum during the winter months and thus further limits the phytoplankton capabilities to make the photosynthesis and to consume the available nutrients. Figure 2.6.2 (a,b) show the correlation coefficient between the monthly time series of $FE_{PO4}$ and $FE_{NO3}$ and the monthly time series of the mixed layer depth (during DJF). The highest correlation values are observed in the Gulf of Lion, Tyrrhenian Sea, Southern Adriatic Sea, Northern Ionian Sea, around Crete and in the area of Rhodes, Pelops and Shikmona gyres, confirming the role of vertical mixing in influencing the distribution of nutrients along the water column. On the other hand, in the coastal areas, the correlation coefficients are weak and negative or even not significant, pointing to the importance of river loads in shaping the variability of nutrients in these areas. In fact, relative lower values of FE are observed in the offshores areas of the basin in December, when the nutrient load from the rivers is prevalent with respect to the injection of nutrients in the euphotic zone from the intermediate/deep layer through vertical mixing (not shown).

The spatial distribution of the relationship between the winter fertilization indicators and the atmospheric drivers is shown in Figure 2.6.3, which reports, for each grid point, the large-scale circulation pattern with the highest value of the difference between $SP^+$ and SPclim for $FE_{PO4}$ and $FE_{NO3}$.

In the case of $FE_{PO4}$, EA is the large-scale circulation pattern driving the variability of potential fertilization indicators in the Western Mediterranean Sea (more specifically in the area of the Gulf of Lion, around the Balearic Island and in the Tyrrhenian Sea) and in the Southern Ionian, around Crete and at centre of the Aegean Sea. In the case of $FE_{NO3}$, we can again observe the same signal in the Gulf of Lion and around the Balearic Island, while it is weaker in the Aegean Sea and completely absent in the Tyrrhenian Sea and Southern Ionian Sea. Tyrrhenian Sea and Southern Ionian Sea are under the influence of the Middle Tyrrhenian current and Atlantic-Ionian stream which results from the bifurcation of the Atlantic Water entering the Mediterranean Sea at the Gibraltar Strait (Pinardi et al. 2015). Thus, it is likely that the boundary conditions set in the Gibraltar Strait play an additional role with respect to the vertical mixing in smearing the variability of $FE_{NO3}$ in the two subbasins. The signal related to EA observed in the Western Mediterranean Sea is in agreement with the findings of previous studies that pointed out the importance of EA in shaping the heat fluxes variability over the region and, in turn, the dense water formation processes and nutrient dynamics in the area (Schroeder et al. 2010; Josey et al. 2011; Reale et al. 2020b). Additionally, EAWR also appears to play an important role for both nutrients in the area of the Rhodes gyre and around Cyprus (Josey et al. 2011; Reale et al. 2020b). No significant relevant signals have been observed in the rest of the basin, in particular in the Southern Adriatic. There, the influence of large-scale circulation patterns is probably masked by the local circulation dynamics (BiOS phenomenon, Gačić et al. 2010; Civitarese et al. 2010). Moreover, the analysis does not show any relevant signal associated with NAO

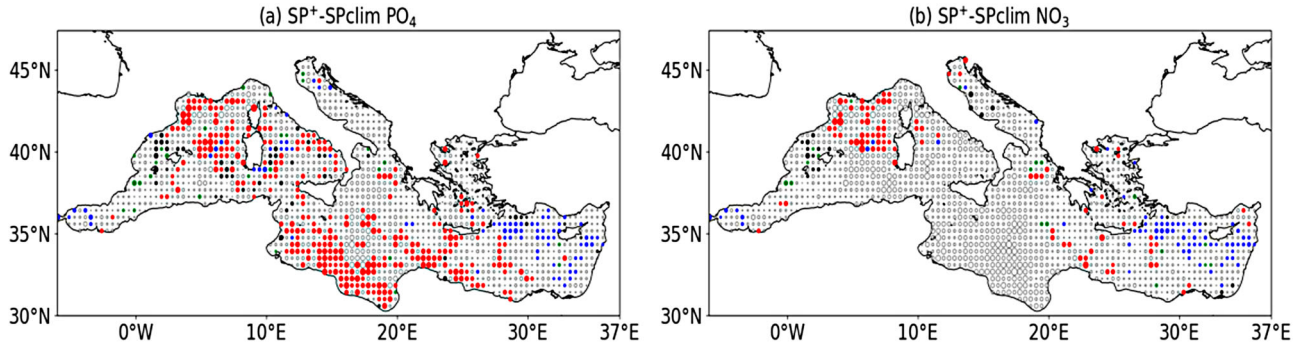


**Figure 2.6.3.** Spatial distribution of the highest value of $SP^+$-SPclim for $PO_4$ (a) and $NO_3$ (b) in the Mediterranean Sea in the period 1999–2019. The size of each dot is equal to the absolute value of $SP^+$-SPclim. The large-scale circulation patterns considered are NAO (black), EA (red), EAWR (blue) and SCAN (green). The resolution of the gridded data has been downgraded from 1/24° to 0.5° for sake of clarity. Values have been computed using the time series of the monthly values of the indexes for large-scale circulation patterns (product reference 2.6.3). Only differences statistically significant with $p < 0.05$ according to a Mann-Withney test are shown.

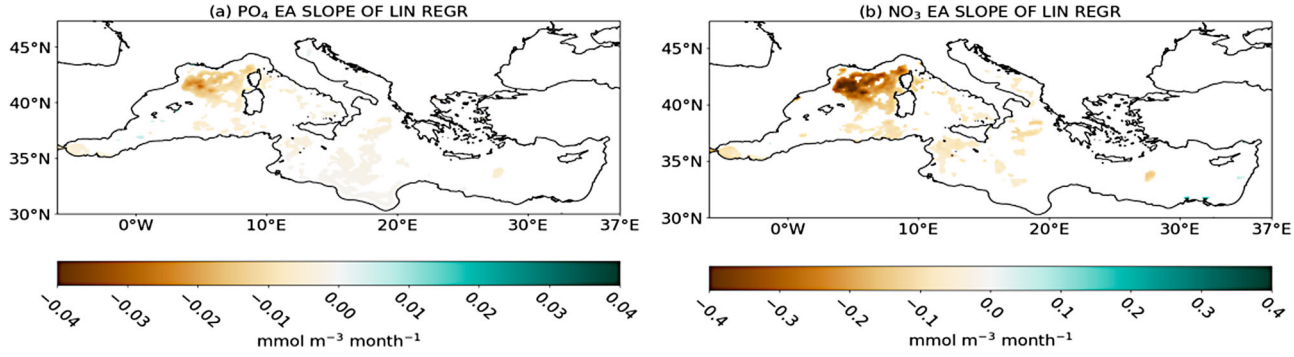


**Figure 2.6.4.** Spatial distribution of the slope of the linear regression between monthly December-January-February time series of $PO_4$ (a) and $NO_3$ (b) and monthly December-January-February EA index time series in the period 1999–2019. Only values statistically significant at 95% are shown. Slopes have been calculated using the CMEMS biogeochemical reanalysis (product reference 2.6.2) and the time series of the monthly values of the indexes for large-scale circulation patterns (product reference 2.6.3)

in the basin, as it is already reported in previous studies (Josey et al. 2011; Reale et al. 2020b).

Figure 2.6.4 shows the slope of the linear regression between the monthly DJF concentration of $PO_4$ and $NO_3$ and the EA monthly index. In fact, provided the existence of a link between the intensity of the fertilization and the atmospheric pattern variability, we assessed the magnitude of this link by computing the regression between the monthly nutrient concentration and that particular large-scale circulation pattern monthly index, with the objective to provide a potential seasonal forecast indicator. The highest values of the slope are observed in the Gulf of Lion area and can get up to $-0.04$ mmol/m$^3$/month and $-0.4$ mmol/m$^3$/month, respectively for $PO_4$ and $NO_3$. The 0–100 m average winter value of $PO_4$ and $NO_3$ amount is equal about 0.2 and 2 mmol/m$^3$ respectively, and the monthly variation of nutrient concentration (in %) for a unit of positive monthly index value of EA is nearly equal to 5%. This estimation is consistent with the results provided in Reale et al. (2020b), who considered the extended winter season October-March (for the past period 1961–1999) and observed a total variation of the nutrient concentration ranging between 2% and 3% for a unit of positive EA index value in the same area. Although long-term analysis (Reale et al. 2020b) and future projections based on CMIP5 models (Ullmann et al. 2014) found no significant tendencies in the EA pattern, the robustness of the link observed mainly in the Gulf of Lion could pave the way to develop seasonal forecasts for the potential fertilization of the area based on the forecast of atmospheric drivers which have become recently available (Lledó et al. 2020).

## 2.6.4. Discussion and conclusions

We introduced an indicator to monitor locally the euphotic layer potential fertilization during the winter season in the Mediterranean Sea and we associated, for each point of the basin, its temporal variability with the large-scale circulation patterns driving the atmospheric circulation over the region. As shown in

Di Biagio et al. (2020), the choice of a specific threshold in each point of the basin allowed us to analyze the potential fertilization in relation to the local ecosystem properties. We found a relevant influence of the EA on the fertilization indicators in the Gulf of Lion. In particular, a negative state of EA results in an increase in the nutrients' concentration in the offshore areas of the Gulf of Lion as well as in the Tyrrhenian Sea, Alboran Sea, Balearic Island, and Southern Ionian Sea (Figure 2.6.4). To a lesser extent, an increase of nutrients' concentration around the Iberian Peninsula, Sardinia, Gulf of Genoa and Northern Adriatic is related to negative EAWR and positive SCAN states. On the other hand, a positive EAWR state corresponds to higher nutrients' concentration in the euphotic layer of the areas around Crete, in the Aegean Sea and the Rhodes Gyre (not shown).

The link observed can be attributed to the importance of EA in shaping the heat fluxes at the surface and thus the vertical mixing along the water column (Josey et al. 2011; Papadopoulos et al. 2012; Reale et al. 2020b). In fact, the vertical mixing acts in such a way to enrich the euphotic layer with nutrients but also to prevent the phytoplankton to concentrate at the surface.

This conclusion is further supported by the spatial distribution of the maximum value of $FE_{PO4}$ and $FE_{NO3}$ during the winter months of 2020 (Figure 2.6.5) which shows a limited fertilization of the euphotic layer of the Mediterranean, in particular in the Northern Western Mediterranean. This limited fertilization appears to be associated with anomalous positive values observed in the EA index in January and February (1.74 and 1.38 respectively).

Only limited significant signals are observed in most of the Adriatic Sea and Aegean Sea where the long-term influence of large-scale circulation patterns on the fertilization indicators is probably masked by the substantial nutrient inflow associated with the presence of the Dardanelles Strait (e.g. Aegean Sea, Souvermezoglou et al. 2014) and local dynamics such as the BiOS phenomenon (e.g. Adriatic and Ionian Sea, Gačić et al. 2010; Civitarese et al. 2010).

Although the approach adopted to derive the indicators could strongly benefit from a longer time series to compute the $90th_{PO4}$ and $90th_{NO3}$ percentiles, the preliminary results are promising, because they provided for the first time an overview of the influence of the atmospheric forcing acting over the Mediterranean region on the interannual variability of the local fertilization in the basin measured by the indicators proposed here. Moreover, the approach adopted here is robust, since it uses physical and biogeochemical assimilated datasets which are based on a physical model forced by the high-resolution atmospheric reanalysis ERA5 (Hersbach et al. 2020). Although the physical and biogeochemical reanalyses contain uncertainty, as described in Escudier et al. (2021) and Cossarini et al. (2021), the use of data assimilation and of ERA5 forcing can contribute to reduce the errors associated with the model's parametrization and boundary conditions, also imposing a constraint on the physics and biogeochemistry of the euphotic layer, and thus providing a better representation of their response to the atmospheric forcing acting over the basin.

Being based on the assessment of the links with the Northern Hemisphere large-scale circulation patterns, the present analysis is focused on one of the possible

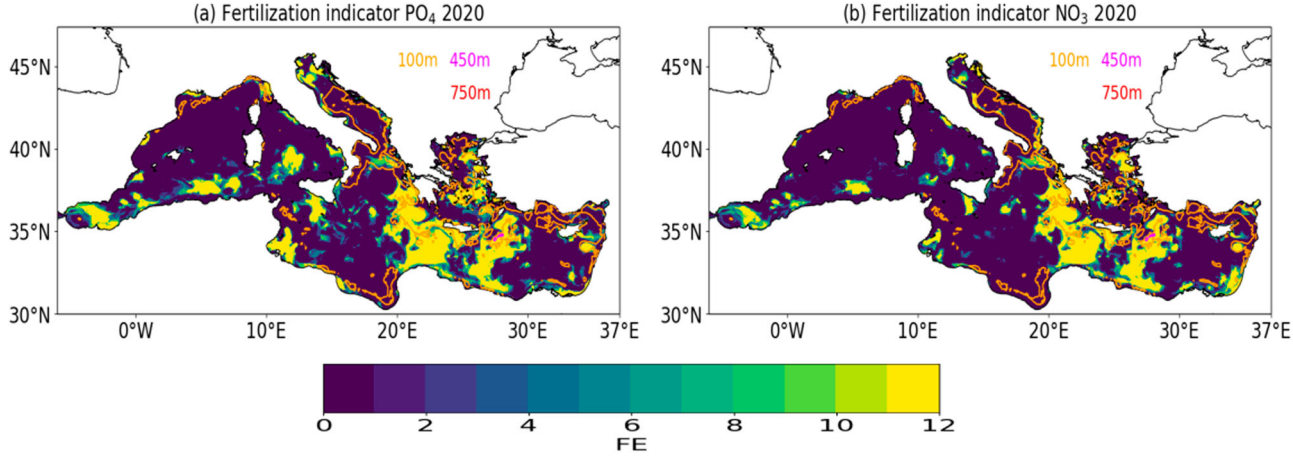


**Figure 2.6.5.** Spatial distribution (in number of days) of the maximum monthly value of $FE_{PO4}$ (a) and $FE_{NO3}$ (b) in the Mediterranean Sea during DJF 2020**.** Contour lines (with colour legend in the figure) shows the mixed layer depth (in m). Mixed layer depth data are based on the CMEMS physical reanalysis (product reference 2.6.1) $FE_{PO4}$ and $FE_{NO3}$ have been calculated using the CMEMS biogeochemical reanalysis (product reference 2.6.2).

fertilization mechanisms affecting the Mediterranean oligotrophic areas. In fact, additional analysis of the riverine inputs, internal dynamics and local mesoscale and sub-mesoscale processes inducing vertical nutrient transport is needed to better understand the variability of the biogeochemical state and the fertilization effects in the euphotic layer of the Mediterranean Sea.

## Acknowledgements

M. Reale has been supported in this work by the project FAIRSEA (Fisheries in the Adriatic Region – a Shared Ecosystem Approach) funded by the 2014–2020 Interreg V-A Italy–Croatia CBC Programme (Standard project ID 10046951).

## Section 2.7. Diversity of marine heatwave trends across the Mediterranean Sea over the last decades

**Authors:** Hugo Dayan, Ronan McAdam, Simona Masina, Sabrina Speich.

**Statement of main outcome:** Over the past three decades, marine heatwaves (MHWs) in the Mediterranean Sea have caused mass-mortality events in various marine species, and critical losses for seafood industries. MHWs are predicted to become more intense and more frequent under anthropogenic warming, embodying a growing threat to both marine ecosystems and human society. To better understand how global warming has led to changes in these events so far, this study assesses past-to-present variability of MHWs in the Mediterranean Sea. Here, we assess the diversity of marine heatwave trends over 1993–2019 across the Mediterranean Sea. Three different surface temperature products show that the maximum intensity, frequency and duration of MHWs have all increased on average over the Mediterranean Sea since 1993. We show that the means of these metrics display a quite inhomogeneous spatial extent across the Mediterranean Sea over 1993–2019, and the trend of these metrics differ between Mediterranean sub-regions. The differences in the changing behaviours of MHW events, depending on the sub-regions, highlight the need for more local-scale risk-assessments and forecasts.

**Product table:**

| Ref. No. | Product name & type | Documentation |
|---|---|---|
| 2.7.1 | SST_MED_SST_L4_REP_OBSERVATIONS_010_021 | PUM: https://marine.copernicus.eu/documents/PUM/CMEMS-SST-PUM-010-021-022.pdf<br>QUID: https://marine.copernicus.eu/documents/QUID/CMEMS-SST-QUID-010-021-022.pdf |
| 2.7.2 | GLOBAL_REANALYSIS_PHY_001_031 | PUM: https://marine.copernicus.eu/documents/PUM/CMEMS-GLO-PUM-001-031.pdf<br>QUID: https://marine.copernicus.eu/documents/QUID/CMEMS-GLO-QUID-001-031.pdf |
| 2.7.3 | MED_MULTIYEAR_PHYS_006_004 | PUM: https://marine.copernicus.eu/documents/PUM/CMEMS-MED-PUM-006-004.pdf<br>QUID: https://marine.copernicus.eu/documents/QUID/CMEMS-MED-QUID-006-004.pdf |
| 2.7.4 | OCEANCOLOUR_MED_CHL_L4_REP_OBSERVATIONS_009_078 | PUM: https://marine.copernicus.eu/documents/PUM/CMEMS-OC-PUM-009-ALL.pdf<br>QUID: https://marine.copernicus.eu/documents/QUID/CMEMS-OC-QUID-009-038to045-071-073-078-079-095-096.pdf |

### 2.7.1. Introduction

In recent years, marine heatwaves (MHWs) – defined as prolonged periods of anomalously high ocean temperature (Hobday et al. 2016) – have drawn attention due to their impacts across the global ocean (IPCC 2014; Oliver et al. 2018, 2021). In the Mediterranean Sea, MHWs have caused ecological and economic damage, such as mass-mortality events and critical seafood losses (e.g. in the summer 1999: Cerrano et al. 2000; Perez et al. 2000; Garrabou et al. 2001; Linares et al. 2005; in the summer 2003: Garrabou et al. 2009; Schiaparelli et al. 2007; Diaz-Almela et al. 2007; Munari 2011; in the summer 2006: Marba and Duarte 2010; Kersting et al. 2013; and in the summer 2008: Cebrian et al. 2011; Huete-Stauffer et al. 2011). The record-breaking 2003 MHW affected the Mediterranean sub-regions differently, particularly impacting benthic populations covering tens to thousands of kilometres of coastlines in the western side of the basin (Garrabou et al. 2009). Over the 1982–2018 period, the basin-averaged Mediterranean Sea SST has displayed a positive trend of 0.41°C/decade, with more rapid warming in the eastern part than in the western part (0.48°C/decade